AD-770 065

EFFECT OF BASE CANT ON CONICAL MARV CONFIGURATION

John W. Ellinwood, et al

Aerospace Corporation

Prepared for:

Space and Missile Systems Organization

December 1967

DISTRIBUTED BY:

NTIS

National Technical Information Service
U. S. DEPARTMENT OF COMMERCE
5285 Port Royal Road, Springfield Va. 22151

Unclassified

Security Classification

DOCUMENT CONTROL DATA - R & D

(Security classification of title, body of abstract and indexing annotation must be entered when the overall report is classified)

1. ORIGINATING ACTIVITY (Corporate author)
Aerospace Corporation
El Segundo, CA

2a. REPORT SECURITY CLASSIFICATION
Unclassified

2b. GROUP

3. REPORT TITLE
Effect of Base Cant on Conical M37 Configuration.

4. DESCRIPTIVE NOTES (Type of report and inclusive dates)
Technical Operating Report

5. AUTHOR(S) (First name, middle initial, last name)
John W. Ellinwood and Robert L. Farwig

6. REPORT DATE
December 1967

7a. TOTAL NO. OF PAGES
23

7b. NO. OF REFS
5

8a. CONTRACT OR GRANT NO.
F04695-67-C-0158

8b. PROJECT NO.

c.

d.

9a. ORIGINATOR'S REPORT NUMBER(S)
TOR-0158(3240-10)-1

9b. OTHER REPORT NO(S) (Any other numbers that may be assigned this report)
SAMSO TR 73-376

10. DISTRIBUTION STATEMENT
Approved for Public Release; Distribution Unlimited.

11. SUPPLEMENTARY NOTES

12. SPONSORING MILITARY ACTIVITY
Space & Missile Systems Orgn (AFSC)
P. O. Box 92960, Worldway Postal Center
Los Angeles, CA 90009

13. ABSTRACT

Theoretical and experimental studies of the effect of a 30° base cant on the pitching moment of a slim conical body have been performed. These analyses have shown that a positive moment due to the base cant is produced for an angle of attack less than the cone half angle. Trim is obtained at angles of attack close to the angle of attack that corresponds to the peak lift-to-drag ratio. The effect on lift and drag is to reduce these quantities approximately by the amount the windward surface area is reduced.

Experimental measurement of the force and moment coefficients, corrected for an anomalous base pressure signal that originated in the test tunnel, verified the theory, at least for sharp-nosed conical bodies. For a model with about 1% blunting, lift and drag coefficients were not essentially different from those of the sharp-nosed body. The observed values of pitching moment were greatly scattered and agreed with the predictions only as to the effects of the base cant. From these predictions and measurements, it is concluded that for slim conical bodies canting the base is a feasible concept for obtaining trim at angles of attack near that corresponding to peak lift-to-drag ratios.

Reproduced by
NATIONAL TECHNICAL
INFORMATION SERVICE
U S Department of Commerce
Springfield VA 22151

ia

DD FORM 1 NOV 65 1473

Unclassified

Security Classification

SAMSO-TR-73-374

AD 770065

Report No. TOR-0158(3240-10)-1

EFFECT OF BASE CANT ON CONICAL MARV CONFIGURATION

Prepared by

John W. Ellinwood and Robert L. Varwig
Aerodynamics and Propulsion Research Laboratory

Laboratory Operations
AEROSPACE CORPORATION
El Segundo, California

Contract No. F04695-67-C-0158

December 1967

Prepared for

SPACE AND MISSILE SYSTEMS ORGANIZATION
AIR FORCE SYSTEMS COMMAND
LOS ANGELES AIR FORCE STATION
Los Angeles, California

DISTRIBUTION STATEMENT A
Approved for public release;
Distribution Unlimited

3AHSO-TR-73-37½

Report No.
TOR-0158(3240-10)-1

EFFECT OF BASE CANT ON CONICAL MARV CONFIGURATION

Prepared by :

John W. Ellinwood

Robert L. Varwig

Approved by

H. Mirels, Head
Aerodynamics and Heat
Transfer Department

R. A. Hartunian, Director
Aerodynamics and Propulsion
Research Laboratory
Laboratory Operations

The information in a Technical Operating Report is developed for a particular program and is therefore not necessarily of broader technical applicability.

ABSTRACT

Theoretical and experimental studies of the effect of a 30° base cant on the pitching moment of a slim conical body have been performed. These analyses have shown that a positive moment due to the base cant is produced for an angle of attack less than the cone half angle. Trim is obtained at angles of attack close to the angle of attack that corresponds to the peak lift-to-drag ratio. The effect on lift and drag is to reduce these quantities approximately by the amount the windward surface area is reduced.

Experimental measurement of the force and moment coefficients, corrected for an anomalous base pressure signal that originated in the test tunnel, verified the theory, at least for sharp-nosed conical bodies. For a model with about 1% blunting, lift and drag coefficients were not essentially different from those of the sharp-nosed body. The observed values of pitching moment were greatly scattered and agreed with the predictions only as to the effects of the base cant. From these predictions and measurements, it is concluded that for slim conical bodies canting the base is a feasible concept for obtaining trim at angles of attack near that corresponding to peak lift-to-drag ratios.

CONTENTS

ABSTRACT iii

I. INTRODUCTION 1

II. THEORY 3

A. Lateral Surfaces, Model II 3

B. Lateral Surfaces, Model I 6

C. Base Effect 8

D. Chord Force Due to Friction 9

III. EXPERIMENTAL MEASUREMENTS 11

A. Application to Present Measurements 14

B. Comparison with Predictions 16

IV. CONCLUSION 20

REFERENCES 21

FIGURES

1. Model Specifications and Dimensions: (a) 30° Canted Base Model I, (b) Adapter to Provide Uncanted Base Model II 2

2. Spherical Quadrilateral 5

3. Sting, Coupling Nut, and Nut Simulator for Base-Pressure Measurements (D = 15.75 – 24.0 in.; d = 8.25 – 24.0 in.) 12

4. Typical Base-Pressure Signals (a) 15.75 in. and (b) 24.0 in. Forward of Coupling Nut 13

FIGURES (Continued)

5. Axial, Forward Normal, and Aft Normal Forces (top to bottom) for MARV Cone Model at $\alpha = 6°$, Base Uncanted. (Average value of deflection normally taken over interval A. To account for base-pressure signal, average deflection over B is used.) 15

6. Force and Moment Distributions for $r_n/L < 0.0007$ 17

7. Force and Moment Distributions for $r_n/L = 0.0123$ 18

I. INTRODUCTION

Employment of slender bodies, and specifically slender cones, for maneuvering reentry vehicle systems has several advantages. Drag can be minimized by the use of moderately sharp-nosed tips, and volumetric efficiency is high. Stability and trim for cone shapes is normally obtained by shifting the center of gravity (c. g.) both axially and laterally. For very slim cones, however, lateral positioning of the c. g. is limited because of the small lateral dimensions. It has been proposed, most recently by AVCO in the MARV concept (Ref. 1), that the required stability and trim can be achieved by canting the base of the vehicle. A pitching moment coefficient C_M that is positive with respect to that of the uncanted-base shape should be produced at small angles of attack α. At angles greater than the cone half angle, the C_M becomes more nearly that of the symmetric cone. Thus, stable trim conditions are obtainable at angles of attack close to that obtained at peak lift-to-drag ratio (L/D).

To evaluate the MARV concept, an experimental study was performed in the Aerospace hypersonic shock tunnel. In this study, aerodynamic forces and moments were measured on two circular cones, one with a 30° canted base and one with a symmetric base (Fig. 1).* Concomitantly, a theoretical analysis was performed to predict pitching moment coefficients for the two shapes. This report contains the analytical method for predicting the moment coefficients and the resulting coefficients. A review of the experimental measurements and a comparison of these results with the theory are also included.

---

*Initial results of this study (Ref. 2) indicated that little difference existed between the two configurations. For a c. g. located 0.675L (L = ref length) aft of the spherical nose, the pitching moment coefficients for the canted-base shape were negative with respect to those of the cone for small α. Further, a value of $C_M = 0$, which corresponds to trim conditions, was never obtained for α other than zero. In view of these apparent discrepancies between the expected behavior and the measured performance, a review of both the theoretical concepts and the experimental procedures was required. Consequently, an examination of the measurement precision and possible systematic errors was begun.

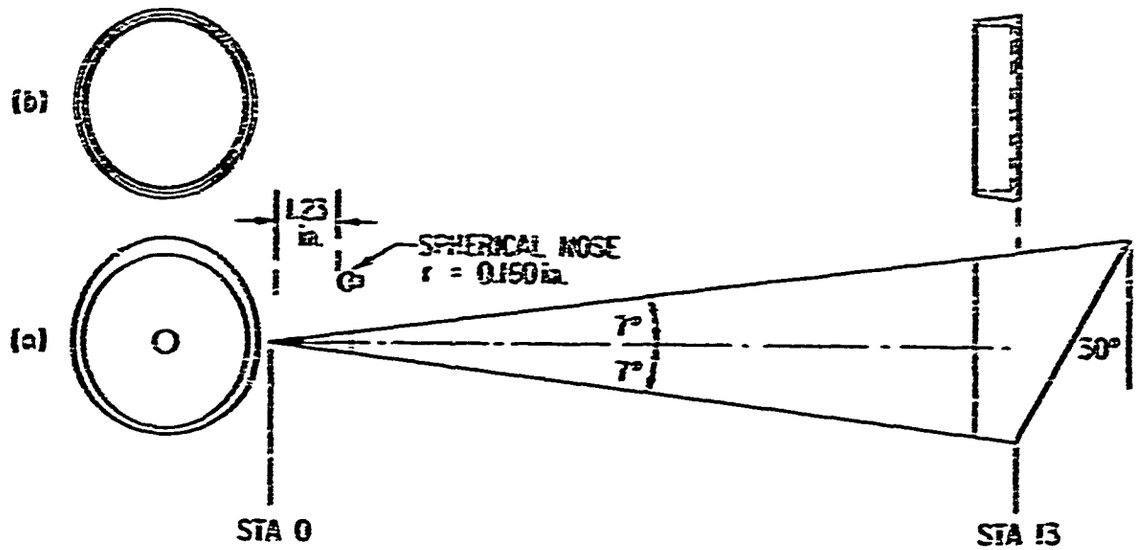

Figure 1. Model Specifications and Dimensions:
(a) 30° Canted Base Model I, (b) Adapter
to Provide Uncanted Base Model II

II. THEORY

Predictions were made for the two sharp-nosed experimental Models I and II shown in Fig. 1. As previously noted, Model I is a 7° half-angle cone with a 30° canted base. Model II is obtained by truncating Model I at station 13 and does not have a canted base.

	Ref. Area, S, ft^2	Ref. Length, L, in.	Moment Center, x_{MC}, in
Model I	0.0744	15	8.8
Model II	0.0556	13	8.8 = 0.676L

A freestream Mach number of 15.8 at a Reynolds number per foot of 2.3×10^5 defines the flow conditions used in the calculations. For both models, the viscous interaction parameter A has a value at the base shoulder of

$$A = \frac{M_\infty^3 \sigma^{-2}}{(Re_{\infty,L})^{1/2}} = \frac{(1.58)^{0.75}(0.123)^{-2}}{\left[2.3 \times 10^5 \left(\frac{13}{12}\right)\right]^{1/2}} = 1.06$$

indicating that the interaction is relatively weak. From Table 3 and Eq. (25) of Ref. 3, the ratio of boundary-layer thickness to local body radius is 0.08 for a freestream stagnation enthalpy ten times the surface enthalpy. The viscous correction consists of replacing the 7° half-angle models by equivalent bodies of half angle $\sigma = 7^{\circ}(1.08) = 7.6^{\circ}$, a procedure that assumes that the boundary layer increase is approximately linear with distance down the body.

A. LATERAL SURFACES, MODEL II

The hypersonic small-disturbance parameter K for zero yaw has the value $K = M_\infty \sigma = 2.1$. From standard tables, the surface pressure coefficient is approximately $2.18\sigma^2$ for air and for this K. We now assume that, with yaw, the surface pressure depends on the local surface incidence σ_* in the same way; i.e., $C_p = 2.18\sigma_*^2$. The dependence of σ_* on the cone angle of attack α, the effective thickness σ, and the local meridian angle ϕ, measured

from the leeward meridian, is found from the spherical quadrilateral ABCD depicted in Fig. 2. From a point O on the model centerline, OA points to the wind, and the sector OBC is part of the model cross section through O that lies between the leeward meridian at B and the local meridian at C. The angles ABC and BCD are both right angles, and OD is the direction of the surface normal. The arc AD then is the complement of $\alpha_{\pm}$, which we seek. Spherical trigonometry leads to the result

$$\alpha_{\pm} = \sin^{-1}\left[-\sin\alpha\cos\sigma\cos\phi + \cos\alpha\sin\sigma\right]$$

With the reasonable assumptions that α^2, σ^2, α^{*2} and related crossproducts can be neglected, we have simply

$$\alpha_{\pm} = \sigma - \alpha\cos\phi + O(\sigma^3)$$

and

$$C_p = 2.18\alpha_{\pm}^2 = 2.18(\sigma^2 - 2\alpha\sigma\cos\phi + \alpha^2\cos^2\phi)$$

For Model II, we integrate C_p from the leeward meridian to the windward meridian to obtain the ratio C_1 of the section normal force to the freestream dynamic pressure.

$$C_1 = -2r(x)\int_0^{\pi} C_p \cos\phi\, d\phi$$

$$= \pm 4.36\pi\, r(x)\sigma\alpha$$

Similarly, the station chord-force coefficient due to pressure is

$$C_d = \frac{2[r(x)]^2}{x}\int_0^{\pi} C_p\, d\phi$$

$$= \pm 4.36\pi\,\frac{[r(x)]^2}{x}\left(\sigma^2 + \frac{\alpha^2}{2}\right)$$

where $r(x)$ is the actual body radius (not the effective body radius). The pitching moment coefficient C_M due to lift is linear in α, neglecting terms

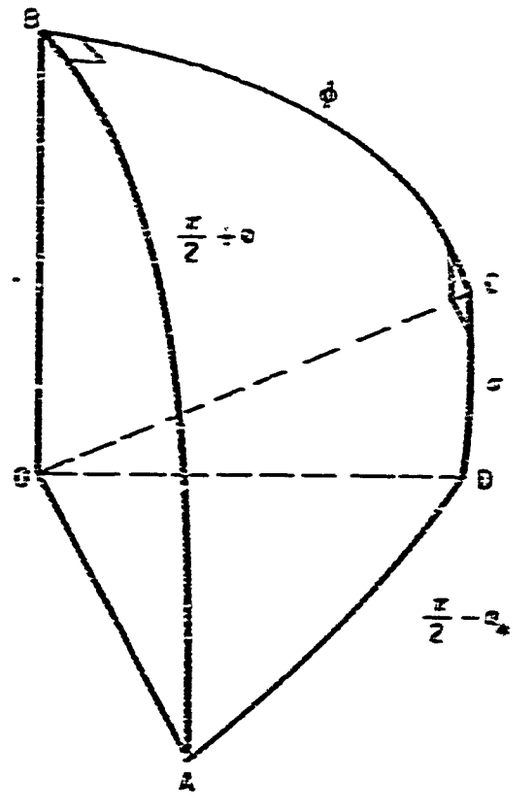

Figure 2. Spherical Quadrilateral

of order $\alpha^2\sigma$, and has the value

$$C_M = -(SL)_{ref}^{-1} \int_{x_i}^{x_f} C_l(x)(x - x_{MC})dx$$

For both models, $x_i = 0$, $x_f = 13$, and $x_{MC} = 8.8$, where the subscript f refers to station 13. Then

$$C_M = 0.0076\alpha\left(\frac{\pi r_f^2}{S_{ref}}\right)\left(\frac{13}{L_{ref}}\right)$$

For Model II, $S_{ref} = \pi r_f^2$ and $L_{ref} = 13$, so that the lateral surfaces of Model II have a C_M due to lift of $+0.0076\alpha$. Similarly, the normal force coefficient is

$$C_N = 2.18(\sigma/7^\circ)\alpha = 2.37\alpha$$

and the pressure chord-force coefficient is

$$C_X = 0.0381\,[1 + \alpha^2/(2\sigma^2)]$$

B. LATERAL SURFACES, MODEL I

The contribution from the sides of Model I differs from Model II in two ways: the reference quantities are different, and there is additional skirt area on Model I due to base cant. The first effect requires multiplying previous results by the ratio $(SL)_{ref,I}$ to $(SL)_{ref,II}$, which is 1.544. The contribution of surfaces forward of station 13 on Model I to C_M is then $+0.0049\alpha$; to C_N, 1.77α; and to C_X, $0.0285\,[1 + \alpha^2/(2\sigma^2)]$.

On the skirt, the local pressure coefficient is as before, but the meridional integration has the upper limit $(\pi/2) + \sin^{-1}\beta$, where

$$\beta(x) = \frac{r_f(\tan 30^\circ) - (x - x_f)}{(\tan 30^\circ)\, r(x)}$$

and $r(x) = r_f + \tan 7^\circ (x - x_f)$. The section force coefficients for $x > 13$ are

$$C_l = -2r(x) \int_0^{(\pi/2) + \sin^{-1}\beta} C_p \cos\phi \, d\phi$$

$$= -4.36r \left\{ \sigma^2 (1 - \beta^2)^{1/2} - \sigma a \left[(\pi/2) + \sin^{-1}\beta - \frac{1}{2} \sin(2 \sin^{-1}\beta) \right] + \frac{a^2}{3} \left[(1 - \beta^2)^{1/2} (2 + \beta^2) \right] \right\}$$

and

$$C_d = 2[r(x)]^2 \int_0^{(\pi/2) + \sin^{-1}\beta} C_p \, d\phi$$

$$= \frac{4.36r^2}{x} \left\{ \sigma^2 [(\pi/2) + \sin^{-1}\beta] - 2\sigma a (1 - \beta^2)^{1/2} + \frac{a^2}{2} \left[(\pi/2) + \sin^{-1}\beta - \beta (1 - \beta^2)^{1/2} \right] \right\}$$

For present purposes, β can be approximated as

$$\beta = 1 - \tau$$

where

$$\tau = (x - x_f)(\cot 30^\circ - \tan 7^\circ)/r_f$$

Then, the moment coefficient due to the skirt is

$$C_M = 4.36(SL)_{ref}^{-1} \int_0^2 (x - x_{MC})\, r \left\{ \sigma^2 (2t - t^2)^{1/2} - \sigma a \left[(\pi/2) + \sin^{-1}(1 - t) - (1 - t)(2t - t^2)^{1/2} + \frac{a^2}{3} \left[(3 - 2t + t^2)(2t - t^2)^{1/2} \right] \right] \right\} dt$$

With the approximation that $r = r_{14}$, we have

$$C_M = \frac{2.18\pi r_{14}}{(SL)_{ref}} \left[(x_i - x_{MC})(\sigma^2 - 2\sigma\alpha + \frac{3}{4}\alpha^2)\right.$$

$$\left. + \frac{r_i}{\cot 33^\circ - \tan 7^\circ}(\sigma^2 - \frac{7}{4}\sigma\alpha + \frac{3}{4}\alpha^2)\right]$$

which for Model I becomes

$$C_M = 0.0072 - 0.1036\alpha + 0.286\alpha^2$$

due to lift on the skirt. The normal force on the skirt is similarly

$$C_N = -0.0193 + 0.290\alpha - 0.820\alpha^2$$

and the chord-force coefficient due to pressure

$$C_X = 0.00475\left(1 - \frac{\alpha}{\sigma} + \frac{\alpha^2}{2\sigma^2}\right)$$

C. BASE EFFECT

The base pressure is assumed to be 3/5 of the freestream pressure for both models. Then on the base,

$$C_p = \frac{-0.4}{\frac{\gamma}{2}(15.8)^2} = -0.0023$$

For Model II, the base pressure contributes only to the base drag coefficient $C_X = 0.0023$. For Model I, the area of the elliptical canted base is 10.8 in.^{2} This is $1.01(S_{ref})$. The moment arm of the force on the base is 2.6 in. or 1.73% of L_{ref}. Hence, C_M due to base pressure is 0.0004, $C_N = -0.0012$, and $C_X = 0.0520$.

I. TOTALS

These results give the following totals for moment, normal force, and chord force due to pressure:

Model I: $C_M = +0.0076 - 0.0937\alpha + 0.285\alpha^2$

$C_N = -0.0205 + 2.06\alpha - 0.820\alpha^2$

$C_X = +0.0404 + 1.08\alpha^2$

Model II: $C_M = +0.0076\alpha$

$C_N = +2.37\alpha$

$C_X = +0.0353 - 0.0361\alpha + 0.943\alpha^2$

D. CHORD FORCE DUE TO FRICTION

For an interaction parameter A of 1.06, for the Prandtl number 0.7, and a cold wall, the skin friction coefficient is

$$C_f = 1.12\left(\frac{p_w}{p_\infty}\frac{C}{Re_{x,\infty}}\right)^{1/2} = 1.12\left(\frac{8}{7}\frac{\gamma M_\infty^2}{2}\frac{C}{Re_{x,\infty}}\right)^{1/2}\left(\frac{C}{p}\right)^{1/2}$$

where the Chapman-Rubesin factor C for a cold wall is

$$C = \left(\frac{T_\infty}{T_r}\right)^{1/4} = \left[\frac{12}{(\gamma - 1)\,Pr M_\infty^2}\right]^{1/4} = 0.643$$

An integration of C_f over ϕ and x leads to a chord force for Model II of

$$C_X = 0.0545 \qquad (\alpha < 7.6^\circ)$$

For Model I, the contribution from stations upstream of 13 is 0.748 times this, or $C_X = 0.0408$, and the contribution from the skirt is

$$C_X = (0.0312)(1.12)\frac{2}{S_{ref}}\int_0^2 r_{14}\int_0^{(\pi/2)+\sin^{-1}\beta}(\sigma - \alpha\cos\phi)d\phi$$

$$= 0.0047\left(1 - \frac{\alpha}{2}\right)$$

I. TOTALS

Where the pressure and friction chord-force contributions are added and the normal force and chord force are converted to lift and drag coefficients, the force results for both sharp-nosed models are

Model I: $C_L = -0.0205 + 1.98\alpha - 0.772\alpha^2$

$C_D = +0.0303 - 0.0589\alpha + 2.96\alpha^2$

Model II: $C_L = 2.275\alpha$

$C_D = +0.0949 + 3.40\alpha^2$

III. EXPERIMENTAL MEASUREMENTS

Experimental measurements of aerodynamic force and moment coefficients were made in the Aerospace hypersonic shock tunnel. Flow Mach and Reynolds numbers were nominally 16 and 2.3×10^5/ft, respectively. These measurements, as indicated in Ref. 2, yielded pitching moment values for the canted base Model I that were negative with respect to those for the symmetric cone Model II. On the other hand, from the preceding analysis one expects a positive pitching moment for a small α for the canted base Model I. If the pressure on the base of the model were much greater than the freestream pressure, then a significant negative moment due to the base cant would be obtained. This moment could contribute to the observed values of C_M for Models I and II. For a cone suspended in the flow without a sting, the base pressure is generally less than the freestream pressure (Ref. 5). Where mounted on a sting that projects from a massive support, this may not be true. There exists the possibility that a pressure wave may propagate upstream along the sting from the bow wave formed ahead of the support.

To examine this hypothesis, base- and surface-pressure measurements were made in the hypersonic shock tunnel on a conical model similar in size and shape to Model II. The cone base-pressure measurements were made in the tunnel at the same location as the force tests of Models I and II. The model and sting arrangement is shown in Fig. 3. The disk mounted on the sting simulates the location of the coupling nut that connects the sting to the support. Base pressures were measured for the same flow conditions ($M = 16$, and $Re/ft = 2.3 \times 10^5$) as those obtained during the force tests. Typical base-pressure measurements are shown in Fig. 4.

When the coupling nut simulator was 8-1/4 in. downstream of the base of the cone, the base pressure (Fig. 4a) rose from a level of $1/2\ p_\infty$ to $5p_\infty$, 3.8 msec after the flow began. When the disk was retracted to 15-3/8 in. from the cone base, no effect on the location (or level) of the base pressure was noted.

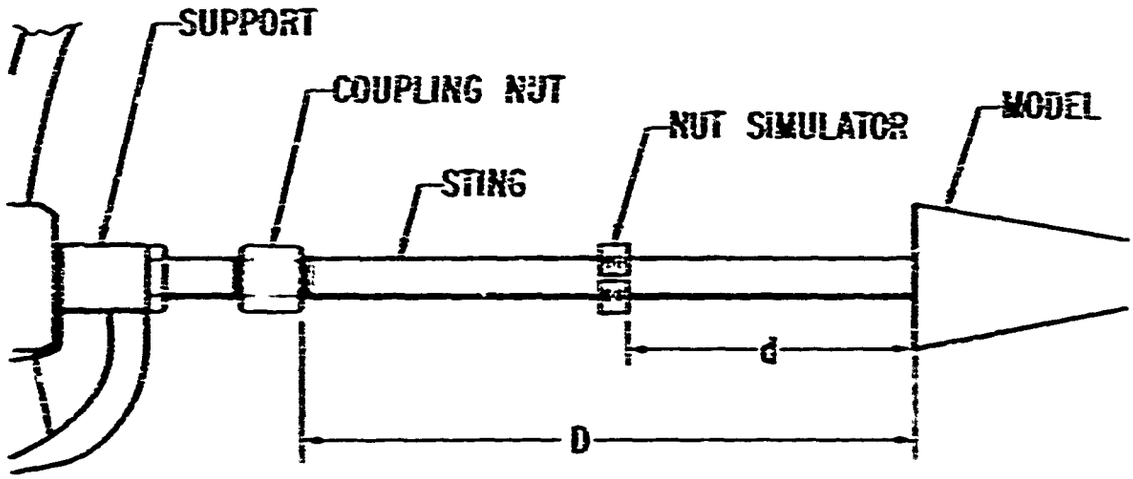

Figure 3. Sting, Coupling Nut, and Nut Simulator for Base-Pressure Measurements (D = 15.75 - 24.0 in.; d = 8.25 - 24.0 in.)

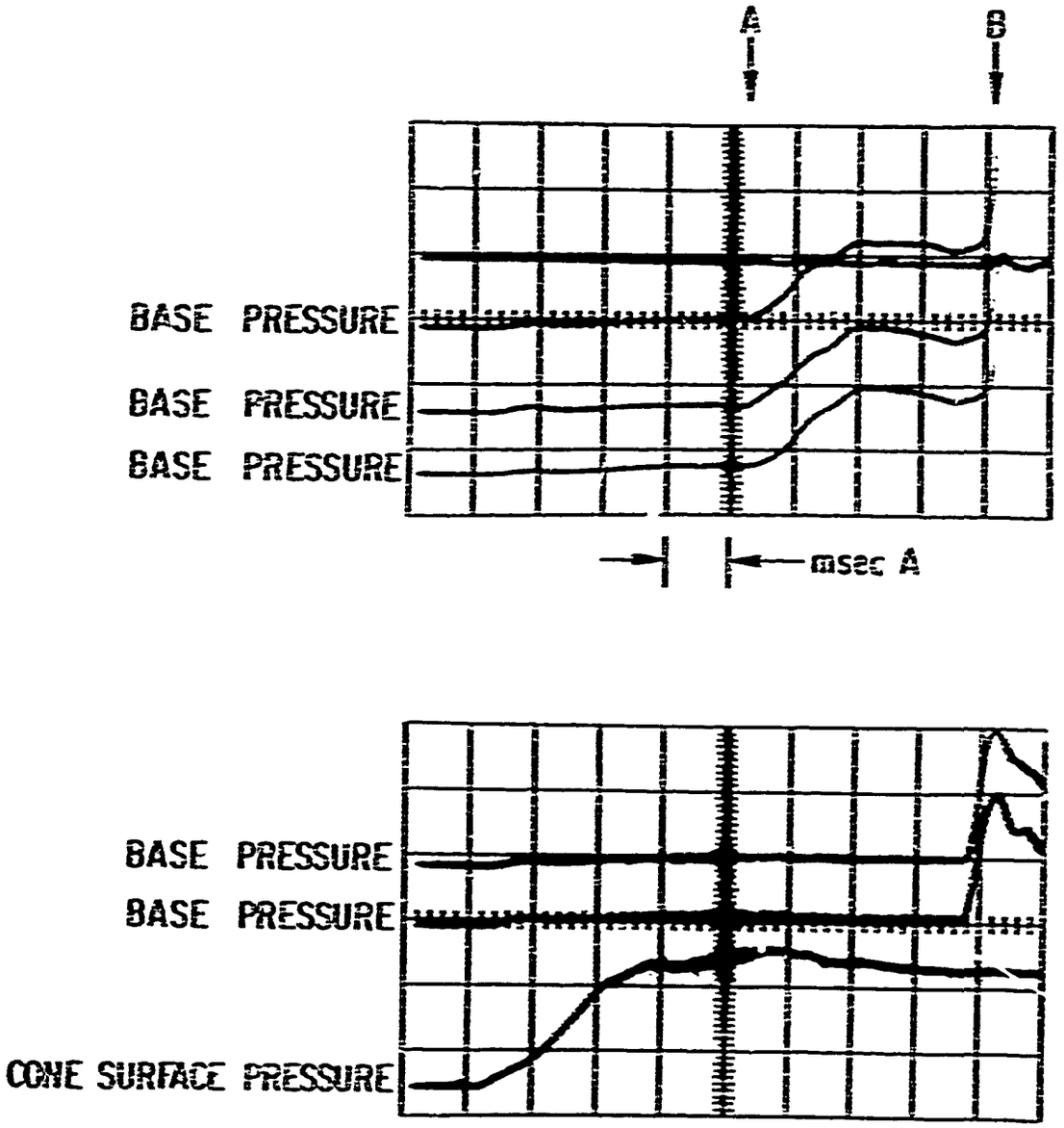

Figure 4. Typical Base-Pressure Signals (a) 15.75 in. and (b) 24.0 in. Forward of Coupling Nut

The cone model was next moved another 8-1/4 in. upstream on the sting, and the coupling-nut simulator was again installed. This time, the base pressure rose from a value of 1/2 p_∞ to 5 p_∞, 7.6 msec after flow started (Fig. 4b). Again, there was no correlation between the arrival time of the 5 p_∞ wave at the base of the model and the location of the coupling nut. Clearly, the base pressure was not a result of a wave moving upstream along the sting. If this were so, the base pressure would have been influenced by the location of the disk on the sting.

Also shown on the base-pressure records of Fig. 4 is the reflected shock wave from the downstream end of the tank, which forms the shock-tunnel test section. Normally, the model is positioned so that this reflected wave arrives at the model at about the same time that the reservoir conditions, influenced by the arrival of the head of the reflected rarefaction wave in the shock tube, begin to decay. This is the optimum test time of a particular tunnel. From records such as these, it was noted that the base-pressure signal travels slightly more slowly than the reflected wave. The approximate origin of the base-pressure signal was determined by extrapolating an x-t curve of its arrival at the two model locations. When this was done, this signal seemed to be originating at the main support for the sting assembly that comes through the sidewall of the tank. The influence of the reflected wave can be eliminated by placing the model far enough upstream in the test section so that the reflected shock wave arrives at the same time, that is, so that this upstream-moving influence does not arrive during the optimum test time. This position is clearly specified by these tests.

It is now required that the farthest downstream element of any force-balance model be at least 2 ft upstream of the sting, i.e., models should be no further downstream than 9-1/2 in. from the contoured nozzle exit.

A. APPLICATION TO PRESENT MEASUREMENTS

Typical traces obtained for Model I and II forces are shown in Fig. 5. The usual way of abstracting the force is to average the signal over the central portion of the record as shown in Fig. 5. This task was complicated by the considerable variation in signal level. Originally, this variation was attributed

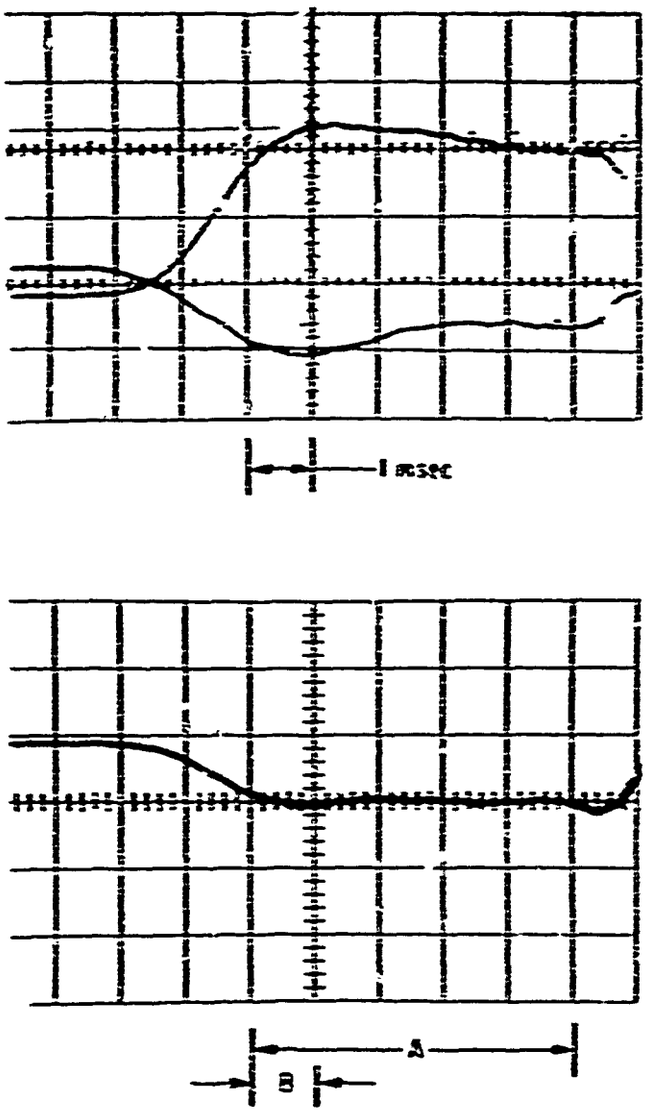

Figure 5. Axial, Forward Normal, and Aft Normal Forces (top to bottom) for MARV Cone Model at $\alpha = 6^{\circ}$, Base Uncanted. (Average value of deflection normally taken over interval A. To account for base-pressure signal, average deflection over B is used.)

to a low-frequency mechanical vibration that the procedure for compensating the force balance had not eliminated. It is now presumed that the variation in the later half of the trace is due to the arrival at the base of the model of the pressure wave now detected. Consequently, it was decided to remeasure the force signals using only the portion of the trace not influenced by the arrival of the base-pressure signal. It should be pointed out that the precision of the data will be adversely affected, and the measurements more scattered. The proper solution is to restrict the test to a region far enough upstream so that the signal does not arrive during the test interval.

The force levels were measured, and the measurements were reduced to force and moment coefficients. The moment center employed is as designated in the theoretical section and is located on the axis 0.675 L of the theoretical cone apex. This position is aft of that defined in Ref. 2 by 0.015 L.

B. COMPARISON WITH PREDICTIONS

Plots of the aerodynamic force and moment coefficients are given in Figs. 6 and 7 for the two nose radii employed. Also on the figures are the values of C_L, C_D, and C_M, predicted from the theory. Predicted and measured drag for the sharp-nosed bodies display the best agreement. For the symmetric cone, the data fall nearly on the theoretical curve for all α. For Model I, drag measurements are within about 10% of the predicted values up to $\alpha = 7^\circ$. The predictions of lift are about as good for Model I as for Model II, high by about 20% in each case. C_M measured for the sharp-nosed Model I is in reasonably good agreement with the predictions for $\alpha < 8^\circ$. Above 8°, the observed value for C_M returns sharply as the canted base skirt drops out of the wind to the value for the symmetric cone. If the predictions had been made for attack angles where part of the surface is leeward, above 8°, it is expected that the predictions would corroborate this return in C_M, although perhaps not as sharply as observed experimentally. Where the predictions apply, the agreement between predicted and observed C_M is good.

For the spherical-nosed models, C_L and C_D are virtually indistinguishable from the sharp-nosed models. The values of C_M are a great deal more scattered, however, and a trend is difficult to detect. As in the case of the

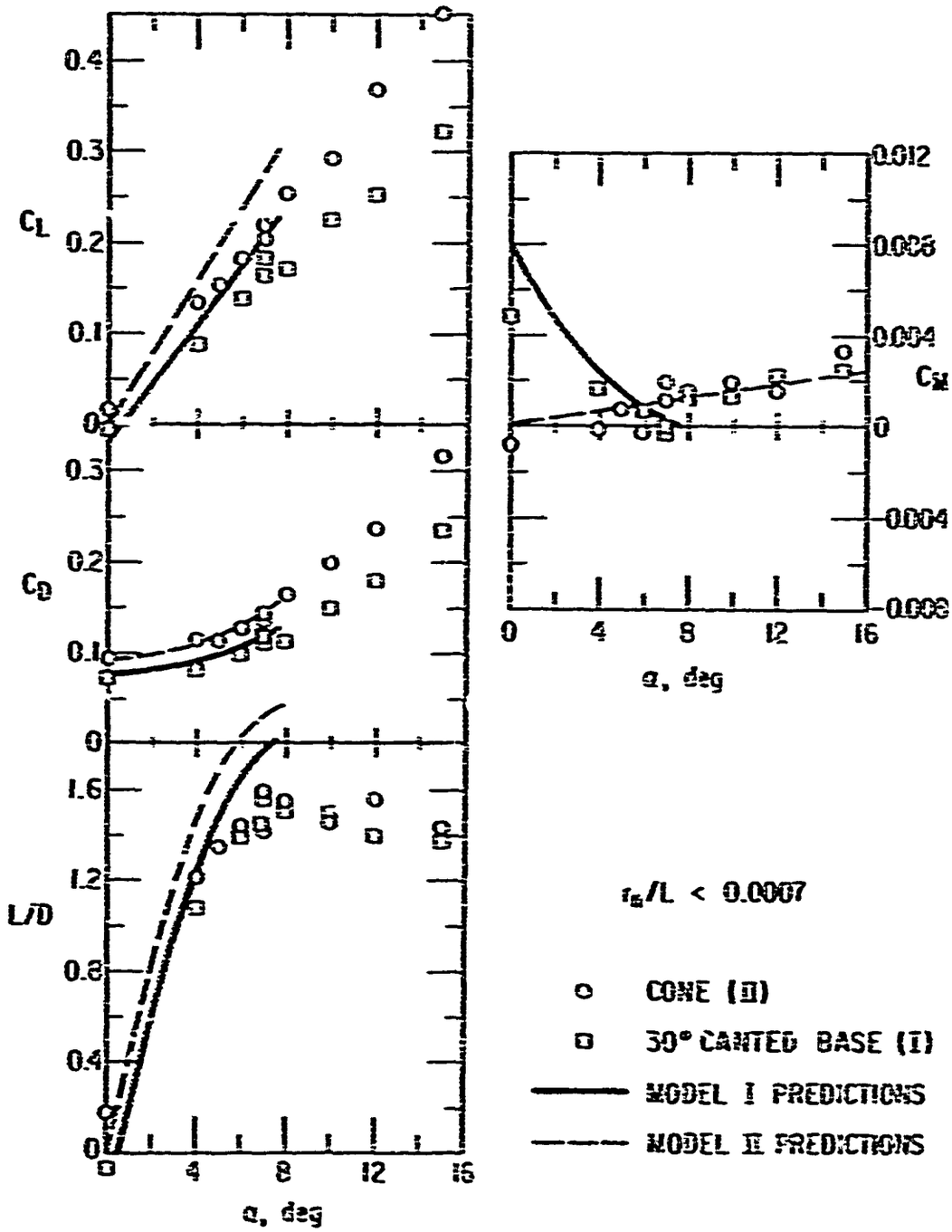

Figure 6. Force and Moment Distributions for $r_n/L < 0.0007$

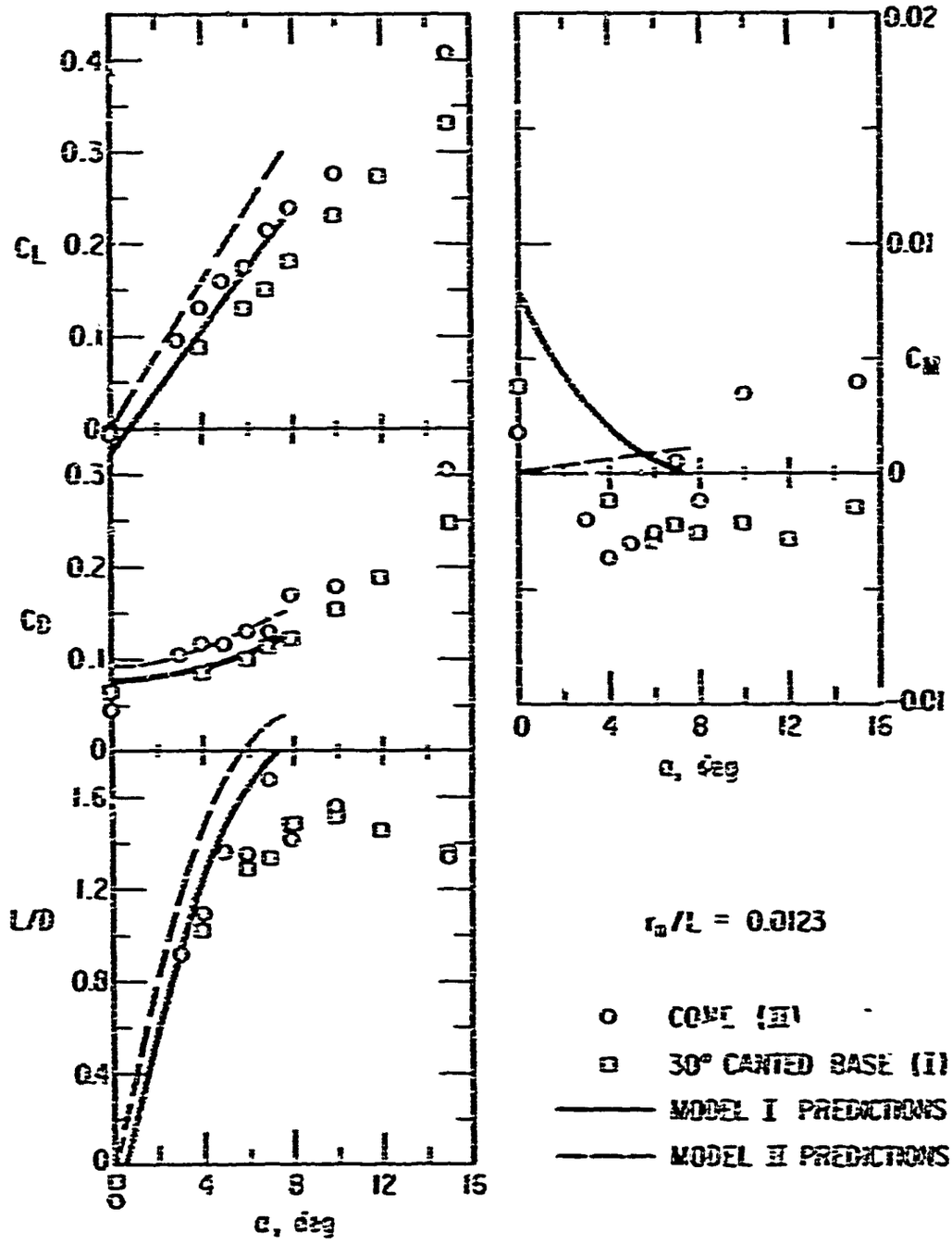

Figure 7. Force and Moment Distributions for $r_n/L = 0.0123$

sharp-nosed models for small α, C_M is positive for the canted-base model with respect to the symmetric-cone model.

Both the predicted and measured values of C_M show that it is possible to trim the model with base cant at angles of attack of interest, i.e., close to that of maximum L/D, thus demonstrating feasibility of the concept.

IV. CONCLUSION

The effect of a 10° base cant on the pitching moment of conical bodies is significant as shown by a theoretical analysis. A positive moment due to the cant is produced for $\alpha < 7^{\circ}$, and trim can be obtained. The effect on lift and drag is to reduce these quantities approximately by the amount the windward surface area is reduced.

Experimental measurement of the force and moment coefficients, corrected for an anomalous base-pressure signal, verified the theoretical results, at least for sharp-nosed conical bodies. For a model with -1% blunting, C_L and C_D were in reasonable agreement with predictions. The observed values of C_M were greatly scattered and, although in quantitatively poor agreement, still agree with predictions as to the effects of the base cant. From these predictions and measurements, one concludes that the base-cant concept is feasible for obtaining trim at values of α close to that corresponding to maximum L/D.

REFERENCES

1. Maneuvering Aerospace Reentry Vehicle Informal Briefing Report, AVCO Space Systems Division, Lowell, Mass.

2. R. L. Varwig and S. B. Mason, Experimental Measurement of the Performance of a 1/10 Scale Model MARV Configuration, TOR-1001 (2240-10)-1 Aerospace Corp. (June 1967).

3. H. Mirels and J. W. Ellinwood, Hypersonic Viscous Interaction Theory for Slender Axisymmetric Bodies, TR-0158(3240-10)-1 Aerospace Corp. (September 1967).

4. D. M. Ellet, Pressure Distributions on Sphere-Cones, SC-RR-64-1795, Sandia Corp., Albuquerque, New Mexico (1965).

5. W. C. Ragsdale and J. A. Darling, An Experimental Study of the Turbulent Wake Behind a Cone at Mach 5, NOLTR 66-95, U. S. Naval Ordnance Laboratory, White Oak, Md. (27 September 1966).